THE JOURNAL OF PHYSICAL CHEMISTRY B

pubs.acs.org/JPCB Article

Sequential Folding of the Nickel/Cobalt Riboswitch Is Facilitated by a Conformational Intermediate: Insights from Single-Molecule Kinetics and Thermodynamics

Hsuan-Lei Sung and David J. Nesbitt*

Cite This: J. Phys. Chem. B 2020, 124, 7348−7360 Read Online

ACCESS | Metrics & More | Article Recommendations

ABSTRACT: The present work presents the first single-molecule fluorescence resonant energy transfer (smFRET) studies of the nickel/cobalt (NiCo) riboswitch, with temperature-dependent, single-molecule confocal microscopy to provide comprehensive kinetic and thermodynamic information on folding into a biochemically competent structure. The results indicate that the NiCo riboswitch first folds into a more compact "prefolded" conformation, with a preorganized binding pocket partially stabilized under physiological conditions by noncognate monovalent/divalent cations. Such a prefolded intermediate then has opportunity to fold further into a tightly ligand-bound structure, in response to the cognate ligands, Ni^{2+} or Co^{2+}, with submicromolar affinities. Such stepwise ligand-induced folding represents a particularly clean example of a conformational selection ("fold-then-bind") mechanism, whereby a configuration dynamically accessible by thermal fluctuation is stabilized into the final folded state by ligand association. In addition, we observe a strong positive cooperativity in the ligand-induced folding kinetics with respect to both Ni^{2+} and Co^{2+} ligands. This provides maximal sensitivity in the riboswitch conformational response near $[Ni^{2+}]$ or $[Co^{2+}] \approx K_d$, which facilitates more accurate biochemical probing of the cell environment and therefore bioregulation of gene expression. Temperature-dependent kinetics at the single-molecule level has also been explored, which permits free energies to be deconstructed into enthalpic and entropic components along the folding coordinate. In the absence of the cognate ligand, a predominantly enthalpic barrier between the unfolded riboswitch (U) and the prefolded intermediate (I) suggests a rearrangement of the hydrogen bonding network, whereas in the presence of the cognate ligand, a large entropic penalty ($-T\Delta S^0 > 0$) in forming the folded riboswitch conformation (F) is almost perfectly counterbalanced by an equivalent enthalpic gain ($\Delta H^0 < 0$) to yield $\Delta G^0 \approx 0$. The thermodynamic results are therefore consistent with a simple physical picture of riboswitch folding, whereby association of the cognate ligand is strongly stabilized by Coulombic attraction while forming an entropically more ordered structure around the binding site.

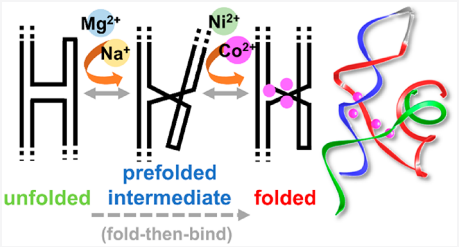

I. INTRODUCTION

Riboswitches are highly structured *cis*-regulatory elements commonly found in the 5′ untranslated region of mRNA.[1,2] Part of the highly conserved structure, known as the aptamer domain, functions as a metabolite sensor that folds to selectively capture the cognate ligand molecule. The rest of the riboswitch sequence comprises the expression platform, which undergoes conformational transitions in response to the aptamer.[2] As a result, the overall riboswitch construct often adopts two mutually exclusive conformations corresponding to "on" and "off" states that structurally regulate expression of the downstream gene.[2,3] Such a regulatory mechanism has been widely exploited in bacteria,[3,4] with riboswitches found to respond to a variety of ligands including small-molecule metabolites and even simple atomic ions.[5]

Heavy metals can be highly cytotoxic, forming complexes with proteins and catalyzing the production of reactive oxidative species damaging to cells.[6,7] However, heavy metals are also essential to cellular function, as they often serve a crucial role in enzymes and enzyme cofactors.[8,9] Ni^{2+}, for example, is a common component of almost all hydrogenases, while Co^{2+} is an essential constituent of vitamin B_{12}. As a result, tight control over intracellular metal ion concentrations is clearly desirable, with sensing and regulatory feedback mechanisms highly evolved to maintain ions at just the right level to support biochemical function while minimizing toxic side effects. In bacteria, for example, genetic expression of membrane transporters and traffic proteins for heavy metals is known to be predominantly controlled by a suite of metalloregulatory proteins.[10,11] The exact role of RNA in maintaining this heavy metal homeostasis is not entirely clear

Received: June 21, 2020
Revised: July 27, 2020
Published: July 27, 2020

https://dx.doi.org/10.1021/acs.jpcb.0c05625
J. Phys. Chem. B 2020, 124, 7348−7360

but changing rapidly. Indeed, the possibility of RNA *selectively responding* to heavy metal ions might at first have been dismissed as unlikely due to the limited types of functional groups available for metal coordination and the well-known association of RNA with physiological Mg^{2+}, the predominant divalent cation in cells.[12,13] By way of contrast, however, riboswitches have recently been identified that respond with remarkably high specificity to manganese (Mn^{2+})[14,15] and nickel/cobalt (Ni^{2+}/Co^{2+}),[16] which in turn regulate the genetic expression of the corresponding protein transporters for these cations. This strongly suggests that metalloregulation is not the exclusive domain of proteins but also cooperatively involves some form of RNA-based sensor of the cellular metal ion environment.

The NiCo riboswitch has been previously referred to as the czcD motif,[16] which resides upstream of czcD genes encoding a subfamily of metal export and resistance proteins.[17−19] The capability of this riboswitch motif for atomic cation Ni^{2+}/Co^{2+} sensing has been recently validated[16] and furthermore confirmed by detection of an explicitly Co^{2+}-bound crystal structure in companion high-resolution X-ray diffraction studies (PDB: 4RUM, Figure 1A). The Ni^{2+}/Co^{2+} sensing

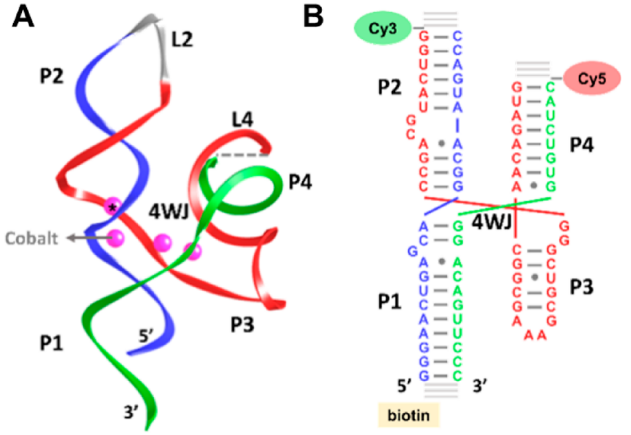

Figure 1. Structure of *E. bacterium* NiCo riboswitch. (A) Overall crystal structure (PDB: 4RUM). (B) Riboswitch sequence in secondary structure representation. The oligomers forming the ternary smFRET construct are indicated in red, green, and blue, respectively.

aptamer domain in this riboswitch consists of a four-way junction, with four helices coaxially stacked in pairs to form a twisted H conformation. As a point of particular relevance to the present study, the NiCo riboswitch construct lacks the long-range tertiary interactions commonly found in other known riboswitches.[16] As a result, the conformation of the junctional loop responds directly to ligand-binding, in turn signaling the on- vs off-state of the gene expression mechanism. Moreover, among the four Co^{2+} ions resolved in the crystal structure (Figure 1A), three form a strong coordination network primarily between the highly conserved guanines at the junction. It is believed that the coordination between Co^{2+} and the guanine nitrogen (N7) provides the source of metal ion selectivity, since Mg^{2+} prefers to coordinate with oxygens in the RNA phosphate backbone rather than nitrogens in the nucleobases.[13,16] In terms of the gene-regulation mechanism, the NiCo riboswitch controls RNA polymerase activity by termination of the transcription event.[16] Upon ligand-binding, the four-way junction, particularly the stem P1, is stabilized by the Ni^{2+}/Co^{2+} coordination network to prevent the expression platform from forming a self-annealed terminator hairpin that in turn disrupts the RNA polymerase transcription complex. As a result, in the presence of excess Ni^{2+}/Co^{2+}, the polymerase complex proceeds to transcribe the mRNA, which encodes for the metal transporter protein.

Riboswitches are highly dynamic in structure with the ability to switch between different conformations in response to ligands to achieve gene regulation.[1] Moreover, upon transcription, the nascent mRNA must fold in real time ($t \approx 1/k_{fold}$) and thereby participate in conformational search over the downstream RNA, a competitive kinetic process known as cotranscriptional folding.[20,21] During transcription, only a limited time window is therefore allowed for the riboswitch to dynamically sample the on- vs off-configurations and thereby achieve the desired ligand response.[22] Consequently, both ligand recognition and conformational folding rates are crucially important to achieving the requisite regulatory effect.[23−25] Over the past decade, single-molecule techniques have been applied to study biomolecular folding and unfolding kinetics. In particular, single-molecule fluorescence resonance energy transfer (smFRET) microscopy has been extensively utilized,[26,27] whereby the conformational change can be visualized in real time by monitoring energy transfer efficiency (E_{FRET}) between the fluorophore pair. Moreover, in contrast to bulk fluorescence measurements where the observed E_{FRET} is averaged over many trillions of replicates, smFRET at the single-molecule level is in principle able to identify multiple conformations from distinct E_{FRET} values to elucidate a more comprehensive folding mechanism.[28−30] Furthermore, precise thermal control is incorporated into the smFRET measurements to facilitate study of the kinetics as a function of temperature. Monitoring the thermal dependence of the NiCo riboswitch kinetics allows us to deconstruct the folding free energies into enthalpic and entropic contributions,[31,32] from which we can generate detailed energy diagrams explicitly demonstrating changes in each of the thermodynamic variables along the folding coordinate.[33,34]

The organization of this paper is as follows. First, the experimental design including the sample preparation and smFRET experimental setup is presented in Section II. Folding of the NiCo riboswitch is then systematically explored at the single-molecule level as a function of (i) monovalent (Na^+), (ii) divalent (Mg^{2+}), and (iii) target ligand (Ni^{2+} and Co^{2+}) cation concentrations as well as (iv) sample temperature, with results presented in Section III. Of particular interest, we find that the NiCo riboswitch exhibits three distinct E_{FRET} states, with a "prefolded" intermediate structure identified to play a crucial role in ligand recognition and riboswitch folding. Such behavior is consistent with a conformational selection ("fold-then-bind") mechanism,[35−37] where the biomolecule spontaneously samples a prefolded structure prior to ligand association and stabilization. This novel combination of (i) stepwise folding and (ii) unique cation response of a riboswitch observed at the single-molecule level is noteworthy and provides material for further discussion in Sections IVA and IVB, respectively. In addition, the thermodynamic variables obtained from our temperature-dependent studies are utilized in Section IVC to reconstruct a detailed free energy diagram of the NiCo riboswitch folding pathway. Finally, Section V summarizes the work and points to directions for future exploration.

https://dx.doi.org/10.1021/acs.jpcb.0c05625
J. Phys. Chem. B 2020, 124, 7348−7360

II. EXPERIMENT

IIA. NiCo Riboswitch Construct Design and Sample Preparation. The aptamer domain of the NiCo riboswitch consists of four helices joined by a four-way junctional loop (see Figure 1).[16] In the cobalt-bound crystal structure (Figure 1A), the two sets of coaxially stacked helices adopt a twisted H conformation with three out of the four resolved Co^{2+} ions in direct contact with the junctional loop. The fourth Co^{2+} ion peripheral to the junction (indicated by * in Figure 1A) shows only relatively low anomalous density in the X-ray diffraction data and appears to make fewer contacts with any of the conserved nucleotides.[16] It is therefore presumed that this final Co^{2+} ion does not play a critical role in NiCo riboswitch folding and might be substitutable by other cations such as physiological Mg^{2+}.

Although not the first example of conformational change in a riboswitch induced by ligand-binding to a junctional loop,[38−40] the NiCo riboswitch is of particular interest in its own right due to two unique structural features:[16] First of all, the suite of three to four Co^{2+} ions occupying the junction loop region and located by anomalous X-ray dispersion data forms a strongly interacting network and suggests that the ligand-binding kinetics may be highly cooperative. Second, the NiCo riboswitch lacks the long-range tertiary interaction motifs and close helical packing, which are relatively common features found in other riboswitches. In combination, this provides a relatively novel opportunity for probing a cooperative ligand-induced conformational response in a riboswitch but probed by the relative orientation between minimally interacting helices.

The NiCo riboswitch in this work is constructed from the *Erysipelotrichaceae bacterium* (*E. Bacterium*) sequence that has been well-characterized in previous study.[16] To achieve surface immobilization and fluorophore labeling, the ternary smFRET construct is assembled by annealing three chemically modified RNA oligomers (Integrated DNA Technologies, Coralville, IA), followed by high-performance liquid chromatography (HPLC) purification, with detailed oligomer sequences and fluorophore-labeled positions illustrated in Figure 1B. (Note: companies are mentioned for explicit information and not by way of commercial product support.) In particular, the P1 stem has been extended by eight base pairs and modified with a terminal biotin to tether the single-molecule RNA construct onto the biotin−BSA surface through biotin−streptavidin interactions. The Cy3 and Cy5 FRET fluorophores are labeled at the distal ends of P2 and P4 (Figure 1B), respectively, corresponding to loops L2 and L4 in the native structure. According to previous structural characterization,[16] L2 and L4 do not respond to ligand-binding and are not part of the conserved sequence essential for ligand sensing and riboswitch function. Thus, we reasonably do not expect our choice of dye labeling sites to interfere with the overall riboswitch conformation. Finally, the distance between Cy3 and Cy5 of the folded NiCo riboswitch is estimated to be $R \approx 45$ Å,[16] which is close to the characteristic Forster length for the Cy3 and Cy5 FRET pair ($R_0 \approx 50$ Å). Due to the extremely rapid ($1/R^6$) dependence of Forster energy transfer, we therefore expect high sensitivity in E_{FRET} values to any changes in the Cy3−Cy5 distance upon conformational unfolding.

To achieve prolonged observation of fluorescent signals from a single RNA molecule, the smFRET NiCo riboswitch constructs are immobilized on the surface of a glass coverslip through biotin−streptavidin interaction. The sample is prepared by successively flushing the sample holder with the following solutions to obtain a typical ∼50 RNA molecules per 100 μm^2 surface coverage:[37,41] (i) 10 mg/mL of bovine serum albumin (BSA) with 10% biotinylated BSA, (ii) 200 μg/mL of streptavidin solution, and (iii) an ∼25 pM (pM = pmole/L) concentration of the smFRET NiCo riboswitch construct, with a 10 min incubation time between each step. Prior to each smFRET experiment, the sample is flushed with an imaging buffer containing (i) 50 mM hemipotassium HEPES buffer (pH 7.5), (ii) a Trolox/PCA/PCD enzymatic oxygen scavenger system to catalytically remove oxygen, (iii) 100 mM NaCl and 0.5 mM $MgCl_2$ to provide background salt (unless otherwise specified), and (iv) sufficient $NiCl_2$ and $CoCl_2$ to achieve desired cation concentration conditions.

IIB. Single-Molecule FRET Spectroscopy and Temperature Control. The single-molecule FRET experiment in this work is based on a home-built confocal microscope system adapted for additional temperature control (Figure 2).[34,41,42]

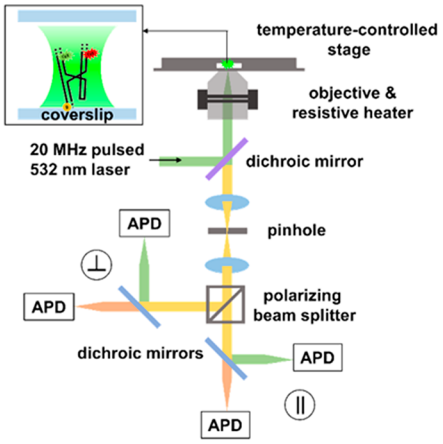

Figure 2. Schematic of the single-molecule confocal fluorescence microscope. Inset: Cartoon representation of a doubly fluorophore-labeled smFRET construct tethered on the surface of a glass coverslip for the single-molecule fluorescence observation.

In brief, a 532 nm collimated beam from a high repetition rate (50 MHz) pulsed Nd:YAG laser is directed onto the sample through an inverted confocal microscope. The beam is tightly focused by a 1.2 N.A. water immersion objective into a diffraction limited laser excitation/collection spot ($1/e^2$ radius ≈ 310(30) nm), allowing for diffraction limited observation of one fluorophore-labeled RNA at a time. The resulting fluorescence photons are collected through the same objective and then separated with dichroics by (i) color (green/red) and (ii) polarization (horizontal/vertical) before detection on single-photon avalanche photodiodes. For each photon detection event, four bits of information (color, polarization, "wall clock" time (sorted into 50 ns bins), and microtime with respect to the laser pulse (50 ps resolution)) are recorded with a fast router, time to amplitude converter (TAC), and time-correlated single-photon counting modules. In this work, we focus primarily on the photon color and arrival time information, with which we can calculate a time-dependent E_{FRET} trajectory.

For temperature-controlled experiments, the temperature is precisely servo loop stabilized by heating the sample and the microscope objective simultaneously.[31,43] Specifically, the

https://dx.doi.org/10.1021/acs.jpcb.0c05625
J. Phys. Chem. B 2020, 124, 7348−7360

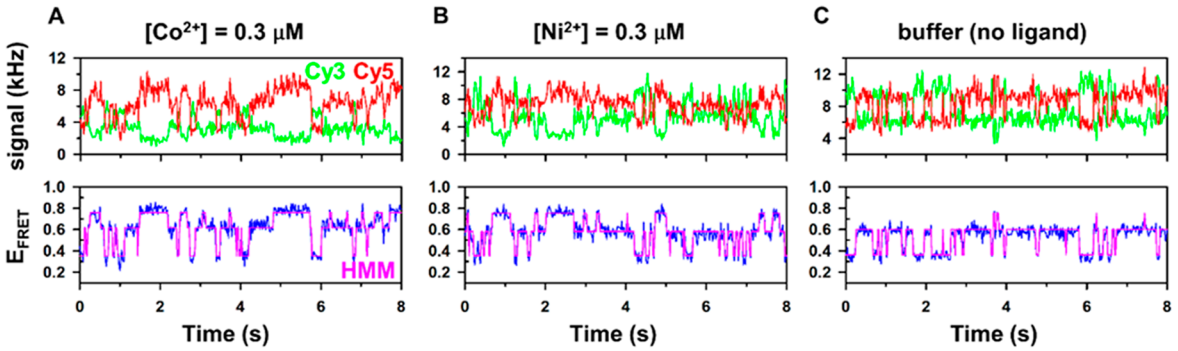

Figure 3. Sample fluorescence time traces of Cy3 and Cy5 signal (upper panel) and corresponding E_{FRET} time trajectories (lower panel) obtained with (A) $[Co^{2+}]$ = 0.3 μM, (B) $[Ni^{2+}]$ = 0.3 μM, and (C) neat buffer (background $[Mg^{2+}]$ = 0.5 mM and $[Na^{+}]$ = 100 mM).

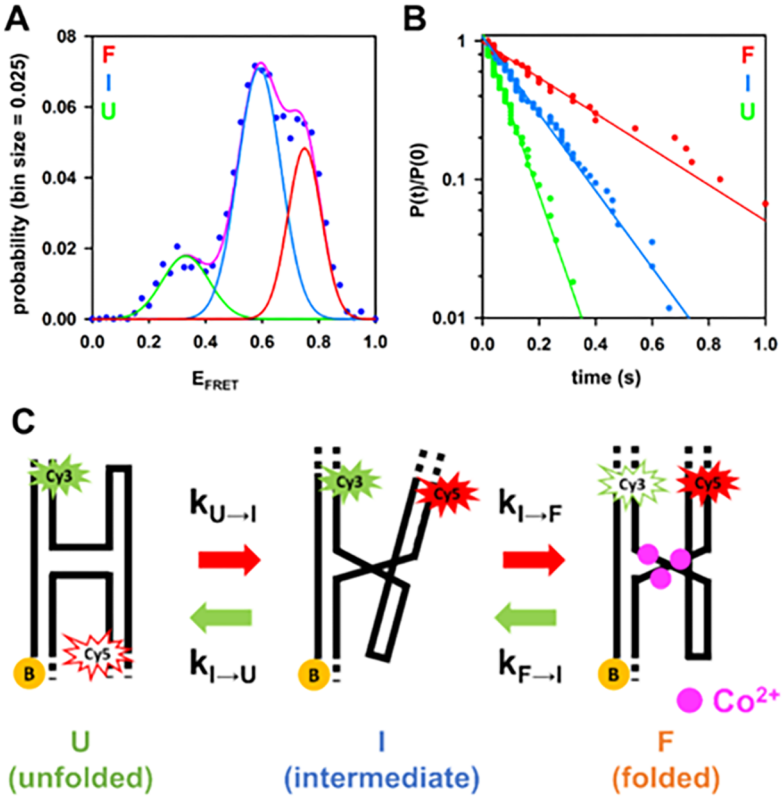

Figure 4. Sample data analysis of the three-state folding system. (A) E_{FRET} histogram fit to three Gaussian functions corresponding to unfolded (U), intermediate (I), and folded (F) subpopulations of the NiCo riboswitch. (B) Exponential decays of the dwell time distributions presented in a semilogarithm plot, indicating that folding and unfolding of the NiCo riboswitch follow first order kinetics. (C) Schematic representation of detailed NiCo riboswitch smFRET construct folding and unfolding. Note that the cartoon representation of the unfolded state (U) suggests a more relaxed/less structured state, which does not necessarily represent the average configuration.

sample holder is mounted to a thermal stage (Instec, Boulder, CO) that regulates the sample temperature by responsive heating and cooling. In addition, a resistive collar (Bioptechs, Butler, PA) is used to simultaneously heat the objective to the desired temperature, minimizing thermal gradients throughout the sample and thereby increasing the servo loop bandwidth and temperature stability. Prior to each experiment, the system is allowed to equilibrate for >15 min to achieve steady sample temperatures with ±0.1 °C precision and accuracy.

IIC. Single-Molecule E_{FRET} Trajectory and Data Analysis. The donor/acceptor fluorescent signals are analyzed with in-house software to generate background and cross talk corrected $E_{FRET} = I(\text{red})/(I(\text{green}) + I(\text{red}))$ trajectories with 20 ms bin time resolution (Figure 3).[31] From visual inspection of sample data in Figure 3, the resulting E_{FRET} trajectories indicate that the NiCo riboswitch exists in three states with distinct E_{FRET} values, which are also clearly evident in the corresponding E_{FRET} histograms (Figure 4A). Due to the fact that the three E_{FRET} distributions are partially overlapping, the traditional methods of dwell time analysis with thresholding prove challenging to implement due to shot noise fluctuations in the fluorescence signals.[31,44] To facilitate the data analysis and improve the reliability of the extracted rate constant information, we have implemented Hidden Markov modeling (HMM) methods based on maximum likelihood estimation, which have been widely applied to study time-dependent single-molecule data.[45−48] Simply summarized, HMM presumes a given kinetic model and optimizes (by changing these

https://dx.doi.org/10.1021/acs.jpcb.0c05625
J. Phys. Chem. B 2020, 124, 7348−7360

model parameters) the likelihood of predicting E_{FRET} values/distributions that correctly match the actual E_{FRET} time trajectory data.[48] Such an approach proves extremely useful in obtaining estimates of E_{FRET} values, number of states, and kinetic rate constants. As one of many powerful attributes, HMM analysis provides access to explicit time trajectory predictions with which to compare to experimental E_{FRET} data (e.g., the dark blue line in Figure 3).

As yet another advantage, HMM analysis allows one to include and rigorously examine the statistical possibility that the system is better described by more than three E_{FRET} distributions.[48] Interestingly, HMM analysis rejects this and consistently predicts three states in the E_{FRET} trajectories (Figure 3, lower panels), corresponding to $E_{FRET} \approx 0.35$, 0.60, and 0.75. The high E_{FRET} state ($E_{FRET} \approx 0.75$) agrees well with our prediction of the folded NiCo riboswitch from the crystal structure.[16] Furthermore, we find virtually all transitions (>98%) between the lowest ($E_{FRET} \approx 0.35$) and highest ($E_{FRET} \approx 0.75$) states exhibit a "pause" at the intermediate $E_{FRET} \approx 0.60$ value, strongly suggesting that the subpopulation with $E_{FRET} \approx 0.60$ corresponds to a folding intermediate (denoted herein as I) that represents a stable transition point between fully folded (F) and unfolded (U) conformations (more details in Section III). We therefore assign the three E_{FRET} populations to be the folded (F, E_{FRET} = 0.75), intermediate (I, E_{FRET} = 0.6), and unfolded (U, E_{FRET} = 0.35) conformations of the NiCo riboswitch, described by a simple kinetic model with four corresponding unimolecular rate constants ($k_{U\to I}$, $k_{I\to U}$, $k_{I\to F}$, $k_{F\to I}$) illustrated schematically in Figure 4C. In Figure 4B, the conventional dwell time analysis of the predicted E_{FRET} trace supports that each folding process is effectively described by a first order rate constant, with the cumulative dwell time distributions well fit to exponential decay functions and yielding HMM predictions of the rate constants summarized in Table I. We can also extend these kinetic results in a few ways. For example, according to the kinetic model, the decay rate constant of the dwell time distribution for state I should be the sum of $k_{I\to U}$ and $k_{I\to F}$ due to parallel I → U and I → F pathways. The individual values of $k_{I\to U}$ and $k_{I\to F}$ can thus be extracted by multiplying the total decay rate constant by the branching ratio for each transition. For instance, the decay rate constant for I is determined to be k = 6.40(12) s^{-1} (Figure 4B, blue line), with numbers of independently observed I → U and I → F transitions as $N_{I\to U}$ = 64 and $N_{I\to U}$ = 21, from which $k_{I\to U}$ and $k_{I\to F}$ can be readily calculated to be 4.82 and 1.58 s^{-1}, respectively. Finally, due to limited statistics on sampling of all three states with limited observation times due to photobleaching, the dwell time data for the HMM analyses are collectively analyzed for each experimental sample run consisting of $N \approx 30$ single molecules separated into n = 3 separate samples. This parsing of the data allows us to obtain HMM rate constants independently for each of the three samples, yielding meaningful statistical averages and standard deviations of the mean.

Table I. Rate Constants Obtained from HMM and Traditional Dwell Time Analysis[a]

	$k_{U\to I}$ (s^{-1})	$k_{I\to U}$ (s^{-1})	$k_{I\to F}$ (s^{-1})	$k_{I\to F}$ (s^{-1})
HMM analysis	13.0	4.90	1.55	2.89
dwell time analysis	13.5(4)	4.82(9)	1.58(4)	3.05(11)

[a]Error bars in parentheses represent 1σ uncertainties from the nonlinear least squares fit.

III. RESULTS AND ANALYSIS

IIIA. Co^{2+}-Promoted NiCo Riboswitch Folding. From previous study of the NiCo riboswitch surveying a wide range of metal cations,[16] the Ni^{2+} and Co^{2+} were alone found to influence the structure of the four-way junction, which in turn correlates with the relative orientation between the four helices. As a result, we can hope to monitor the effects of Ni^{2+}- and Co^{2+}-binding to the four-way junction loop via time-dependent E_{FRET} trajectories (Figure 3). Since the Co^{2+} ion positions are most clearly resolved from X-ray crystal structures,[16] we first systematically explore the folding kinetics of the NiCo riboswitch as a function of [Co^{2+}]. Specifically, HMM methods are used to analyze E_{FRET} trajectories for a statistically significant sample (three independent sets of $N \approx$ 10 molecules) of NiCo riboswitch constructs, to obtain the four kinetic rate constants ($k_{U\to I}$, $k_{I\to U}$, $k_{I\to F}$, $k_{F\to I}$) connecting the unfolded (U), intermediate (I), and folded (F) conformational manifolds. The results from such an analysis are summarized in a plot of rate constants (Figure 5A) as a function of Co^{2+}, with the equilibrium fraction of U, I, and F states at each ion concentration depicted in Figure 5B. From the bottom panel, it is clear that the overall complex equilibrium shifts systematically from unfolded (~(U + I)) to predominantly folded (~ F) at increasing [Co^{2+}] with submicromolar affinities. However, parsed in terms of individual rate constant contributions, the kinetics become

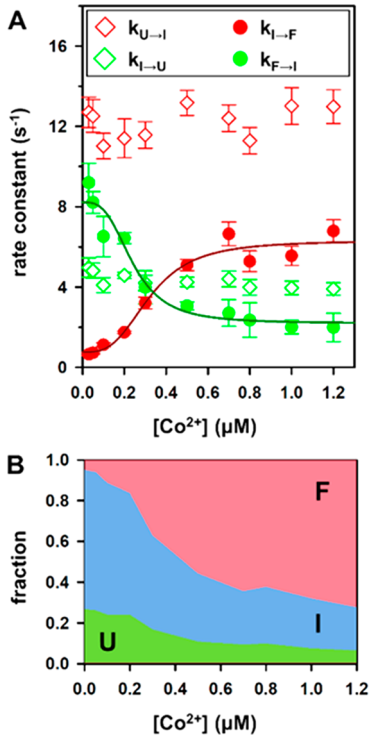

Figure 5. Co^{2+} dependence of NiCo riboswitch folding. (A) Rate constants $k_{U\to I}$ (red empty diamonds), $k_{I\to U}$ (green empty diamonds), $k_{I\to F}$ (red solid circles), and $k_{F\to I}$ (green solid circles) as a function of [Co^{2+}]. (B) Equilibrium fraction as a function of [Co^{2+}] (green: U, blue: I, red: F). Solid lines represent fits to the Hill equation (eq 1). Error bars represent 1σ standard deviations of the mean.

https://dx.doi.org/10.1021/acs.jpcb.0c05625
J. Phys. Chem. B 2020, 124, 7348−7360

even more interesting, as displayed in Figure 5A. For example, the major contributor to such conformational transformation appears to be the forward/reverse rate processes between I and F (solid circles), with the successful folding of the NiCo riboswitch (U → F) promoted by a simultaneous $[Co^{2+}]$-dependent *increase in* $k_{I\to F}$ (I → F transition) and *decrease in* $k_{F\to I}$ (F → I transition), respectively. Of particular relevance, the rate of increase in $k_{I\to F}$ for low $[Co^{2+}]$ is *supralinear*, which suggests that conformational change from I to F is driven by the *cooperative* presence of multiple Co^{2+} ions.[49] This can be further quantified by least-squares fits of the rate constants to a Hill equation[37,50,51]

$$k_{I\to F} = k_0 + (k_1 - k_0)\left(\frac{[M^{2+}]^n}{K_d{}^n + [M^{2+}]^n}\right) \quad (1)$$

where k_0 represents the value of $k_{I\to F}$ at $[Co^{2+}] = 0$, k_1 represents the saturated value of $k_{I\to F}$ at high $[Co^{2+}]$, K_d is the apparent dissociation constant, and n is the Hill coefficient. The fits yield a Hill coefficient of $n = 3.1(11)$ for Co^{2+}-promoted folding (Table II), again indicating a strong positive cooperativity and in good agreement with previous in-line probing assays.[16] Conversely, the unfolding rate constant $k_{F\to I}$ decreases as a function of increasing $[Co^{2+}]$. Since the range of $[Co^{2+}]$ explored (0 to 1.2 μM) is 2 to 3 orders of magnitude lower than the background $[Mg^{2+}]$ (~0.5 mM), this monotonic decrease in $k_{F\to I}$ cannot result from purely cationic stabilization of the aptamer domain by Co^{2+}. Indeed, $k_{F\to I}$ has already been shown (Section IIIC) to be insensitive to $[Na^+]$ and $[Mg^{2+}]$ in the absence of Ni^{2+} or Co^{2+}, which indicates that $k_{F\to I}$ primarily depends on ligand association. Thus, the strong dependence of $k_{F\to I}$ on $[Co^{2+}]$ suggests that the NiCo riboswitch unfolds at distinctive rates from each subpopulation (F_i) with different numbers of Co^{2+} ions and with the equilibrium between each state $F_{i=1,2,3}$ modulated by $[Co^{2+}]$,[37] thus naturally leading to a strongly $[Co^{2+}]$-dependent unfolding. In order to model the decrease in $k_{F\to I}$ with Co^{2+}, the kinetic data in Figure 5A are similarly fit to the Hill equation (eq 1) with n fixed at a 3.1 value from the analysis of $k_{I\to F}$ (Table II).

Table II. Fitting Results from Hill Analysis

	k_0 (s^{-1})	k_1 (s^{-1})	K_d (μM)	n
$k_{I\to F}$ (Co^{2+})	0.8(3)	6.3(5)	0.32(4)	3.1(11)
$k_{F\to I}$ (Co^{2+})	8.2(4)	2.2(3)	0.24(3)	3.1[a]
$k_{I\to F}$ (Ni^{2+})	0.9(2)	2.6(2)	0.26(7)	1.8(10)
$k_{F\to I}$ (Ni^{2+})	7.7(8)	1.8(4)	0.17(6)	1.8[a]

[a](Indicates parameters fixed in the fit). Error bars in parentheses represent 1σ uncertainties from the nonlinear least squares fit.

By way of contrast, the conformational kinetics sampling transitions between the unfolded (U) and intermediate (I) states is insensitive to $[Co^{2+}]$ (Figure 5A, empty diamonds), with $k_{U\to I} \approx 13\ s^{-1}$ and $k_{I\to U} \approx 4\ s^{-1}$, respectively. This implies that the NiCo riboswitch is actively sampling the "prefolded" intermediate state with a similar rate constant under all buffer conditions here. As these "prefolding" rate constants are on the order of or larger than the subsequent (I → F) folding rate constants, the fractional split between [U] and [I] (see Figure 5B) remains relatively constant over the full dynamic range of $[Co^{2+}]$ explored. However, since I folds efficiently upon Co^{2+}-binding, the overall concentration [U + I] is significantly depleted with increasing $[Co^{2+}]$ as the overall equilibrium is driven toward [F] (Figure 5B).

IIIB. Ni^{2+}-Promoted NiCo Riboswitch Folding. The NiCo riboswitch has been shown to respond to Ni^{2+} as well as Co^{2+} in previous structural studies and *in vitro* transcription assays.[16] Although the X-ray crystal structure of the Ni^{2+}-bound NiCo riboswitch is currently unavailable, previous in-line probing studies have revealed similar cleavage patterns in response to Ni^{2+} and Co^{2+} ions, suggesting that both ligands induce a similar conformational change. Experimentally (see Figures 3 and 6), the present studies show remarkably similar single-molecule folding kinetics as a function of either $[Ni^{2+}]$ or $[Co^{2+}]$. For example, time-dependent E_{FRET} trajectories for the NiCo riboswitch construct in the presence of Ni^{2+} (Figure 3) also exhibit three distinct states (U, I, and F), indeed with the same E_{FRET} values (0.35, 0.6, 0.75) seen in the presence of Co^{2+}. Also consistent with the $[Co^{2+}]$ dependence, the rate constants for folding ($k_{U\to I}$) and unfolding ($k_{I\to U}$) from U to the "prefolded" intermediate I remain relatively constant over the range of $[Ni^{2+}]$ studied (Figure 6A, empty diamonds), with the equilibrium driven toward the F conformation by a simultaneous increase and decrease in $k_{I\to F}$ and $k_{F\to I}$, respectively (Figure 6A, solid circles). The only quantitative differences in the rate analyses can be seen in the Ni^{2+} vs Co^{2+} dependence of $k_{I\to F}$. Specifically, $k_{I\to F}$ increases less supralinearly with $[Ni^{2+}]$ than $[Co^{2+}]$, which is consistent with a lower (albeit finite) Hill cooperativity and a significantly lower saturation rate constant in $k_{I\to F}$. Indeed, least-squares Hill fits of k_0, k_1, K_d, and n to eq 1 yield $k_0 = 0.9(2)\ s^{-1}$, $k_1 = 2.6(2)\ s^{-1}$, $K_d = 0.26(7)\ \mu$M, and $n = 1.8(10)$, respectively (Table II).

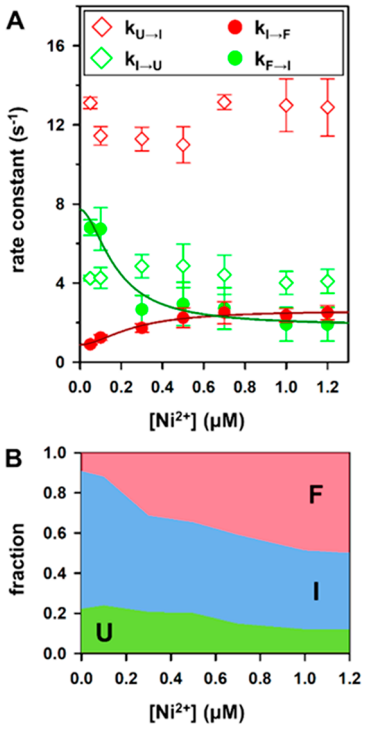

Figure 6. Ni^{2+} dependence of NiCo riboswitch folding. (A) Rate constants $k_{U\to I}$ (red empty diamonds), $k_{I\to U}$ (green empty diamonds), $k_{I\to F}$ (red solid circles), and $k_{F\to I}$ (green solid circles) as a function of $[Ni^{2+}]$; (B) equilibrium fraction as a function of $[Ni^{2+}]$ (green: U, blue: I, red: F). Solid lines represent fits to the Hill equation (eq 1). Error bars represent 1σ standard deviations of the mean.

https://dx.doi.org/10.1021/acs.jpcb.0c05625
J. Phys. Chem. B 2020, 124, 7348−7360

Note that Ni^{2+}-promoted folding of the NiCo riboswitch construct still exhibits positive cooperativity ($n > 1$), though with lower levels than Co^{2+}.[16]

IIIC. Physiological Cation (Na^+/Mg^{2+}) Effects on the NiCo Riboswitch Structure. Counterions (cations) are essential for RNA folding due to charge neutralization and electrostatic screening.[52,53] Cations in the cellular environment are quite abundant, with monovalent (Na^+ and K^+) and divalent (Mg^{2+}) cation concentrations at the ~100 and few mM levels, respectively. It is thus useful to probe NiCo riboswitch conformational kinetics and dynamics under physiological cation conditions in the complete absence of a Ni^{2+} or Co^{2+} cognate ligand. We first explore the NiCo riboswitch as a function of $[Na^+]$ without divalent cations, i.e., $[Mg^{2+}] = 0$ (Figure 7A). It is important to note that we still see

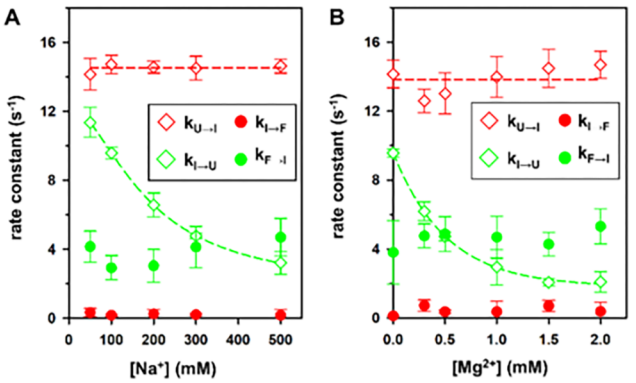

Figure 7. General monovalent/divalent background cation dependence of NiCo riboswitch folding. Rate constants $k_{U\to I}$ (red empty diamonds), $k_{I\to U}$ (green empty diamonds), $k_{I\to F}$ (red solid circles), and $k_{F\to I}$ (green solid circles) are studied as a function of (A) $[Na^+]$ and (B) $[Mg^{2+}]$ concentration. Dashed lines are added to highlight the change in k (or lack thereof) as a function of cation concentration. Error bars represent 1σ standard deviations of the mean.

clear evidence in the E_{FRET} trajectories for the three conformational states (U, I, and F) even in the absence of ligands (see Figure 3C), which indicates the robustness of the prefolded intermediate and motivates a similar HMM analysis of the rate constants (see Figure 7A,B). Interestingly, three of the four rate constants show little dependence on monovalent $[Na^+]$, with the only significant response that the rate constant for unfolding of the intermediate ($k_{I\to U}$) is reduced by Na^+ (Figure 7A). Stated alternatively, an increase in $[Na^+]$ primarily enhances the fractional concentration of the prefolded intermediate [I]/[U] by *decelerating* the rate of I → U *unfolding*. This is in dramatic contrast to the behavior noted previously for the cognate ligand cations, which impact only the rate constants for final folding from I to F ($k_{I\to F}$) or vice versa ($k_{F\to I}$) with negligible impact on the corresponding U to I initial folding/unfolding steps ($k_{I\to U}$ and $k_{U\to I}$). Also surprisingly, the high E_{FRET} folded state (F) is observable over the entire range of $[Na^+]$ explored, though formed with a much lower rate constant (i.e., $k_{I\to F} \approx 0.2\ s^{-1}$) and equilibrium probability ($K_{I\leftrightarrow F} \approx 0.05$), with both $k_{I\to F}$ and $k_{F\to I}$ exhibiting no systematic dependence on $[Na^+]$. These results indicate that the NiCo riboswitch can dynamically sample the fully folded conformation even without cognate ligand-binding to stabilize the final biochemically competent state.

Similar effects are also observed in studies of the Mg^{2+}-dependent folding/unfolding kinetics at a constant monovalent background $[Na^+]$ = 100 mM (Figure 7B), except that reduction in the unfolding rate constant ($k_{I\to U}$) is now >100-fold more sensitive to Mg^{2+} and responds at the submillimolar level. Therefore, both Na^+ and Mg^{2+} background levels efficiently promote the intermediate population (I) by decelerating the unfolding rate constant $k_{I\to U}$ without a significant impact on unimolecular folding to the final folded state $k_{I\to F}$. A differential response to the two cationic species and cognate ligands in terms of folding of the NiCo riboswitch may therefore be sorted into two separate contributions (see Figure 4): (i) prefolding from U to I promoted by universal (i.e., nonselective) counterion stabilization effects (both Na^+ and Mg^{2+}) and (ii) folding from I to F promoted by selective cognate ligand-binding. Although Na^+ and Mg^{2+} do not by themselves promote the fully folded state (F), they do nevertheless facilitate formation of the NiCo riboswitch by encouraging a "fold-like" conformation (I) and effectively suppressing the unfolded state (U). As a result, the overall fraction of the fully folded state can still be enhanced by background $[Na^+]$ and $[Mg^{2+}]$. We note that such cation effects to promote a fold-like state in preparation for folding have been observed in multiple riboswitch systems with Mg^{2+}.[29,36,37] It is also not surprising that cations like Na^+ yield stabilization effects at higher concentration, as monovalent-ion-promoted folding has been demonstrated with fundamental RNA tertiary folding motifs such as the kink turn,[54] four-way junction,[55] and tetraloop receptor[44,56] commonly found in fully functional RNA.

IIID. Temperature-Dependent Folding Equilibrium: Van't Hoff Analysis. Temperature has a significant impact on biomolecular structure, as the folding/unfolding kinetics depend exponentially on enthalpic and/or entropic contributions to the overall free energy differences. Indeed, the temperature dependence of biomolecular folding contains crucial thermodynamic information that helps provide a clearer physical picture of the folding dynamics.[33] Toward that end, NiCo riboswitch folding kinetics at the single-molecule level has been studied as a function of temperature ($T \approx 20-30$ °C), with and without the primary cognate ligand ($[Co^{2+}]$ = 0.0 and 0.5 μM), and analyzed by HMM methods as described in Section IIC. As a first stage of analysis, we focus on the two temperature-dependent equilibrium constants, $K_{U\leftrightarrow I}(T) = k_{U\to I}/k_{I\to U} = [I]_{eq}/[U]_{eq}$ and $K_{I\leftrightarrow F}(T) = k_{I\to F}/k_{F\to I} = [F]_{eq}/[I]_{eq}$, which are extracted from the HMM modeling and displayed in a conventional van't Hoff plot in Figure 8. This allows us to deconstruct the two folding free energy differences (U → I and I → F) into changes in enthalpy (ΔH^0) and entropy (ΔS^0) via a linear fit to the standard van't Hoff expression

$$\ln(K_{eq}) = -\frac{\Delta H^0}{R}\frac{1}{T} + \frac{\Delta S^0}{R} \qquad (2)$$

In the absence of Co^{2+} (Figure 8A) $K_{U\leftrightarrow I}$ shows only a weak dependence on the temperature (i.e., slope $m \approx 0$ within experimental uncertainty), indicating therefore a negligible enthalpic contribution ($\Delta H^0_{U\to I}$ = 1.4(13) kcal/mol ≈ 0). Conversely, we can extrapolate eq 2 in the high-temperature limit to yield a positive intercept that reveals U → I folding to be dominated by only modest entropic gain ($\Delta S^0_{U\to I}$ = 7(4) cal/mol/K). The second stage (I ↔ F) folding equilibrium constant ($K_{I\leftrightarrow F}$) exhibits a more pronounced dependence on

https://dx.doi.org/10.1021/acs.jpcb.0c05625
J. Phys. Chem. B 2020, 124, 7348−7360

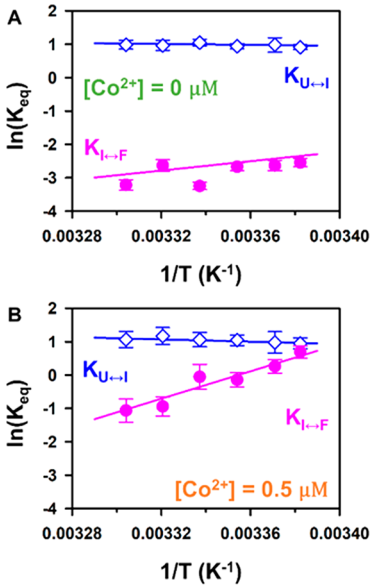

Figure 8. Temperature dependence of equilibrium constants presented in van't Hoff plots at (A) $[Co^{2+}]$ = 0 μM and (B) $[Co^{2+}]$ = 0.5 μM (blue empty diamonds: $K_{U\leftrightarrow I}$, pink solid circles: $K_{I\leftrightarrow F}$). Data fits with linear regression yield detailed thermodynamic information (i.e., ΔH^0 and ΔS^0) by eq 2. Error bars represent 1σ standard deviations of the mean.

temperature, now with an overall positive slope consistent with a mildly exothermic process ($\Delta H^0_{I\to F}$ = −14(8) kcal/mol) and a negative intercept indicating an overall entropic penalty to folding ($\Delta S^0_{I\to F}$ = −52(26) cal/mol/K). Thermodynamic data obtained from these van't Hoff analyses are summarized in Table III.

In the presence of 0.5 μM Co^{2+} (Figure 8B), the temperature dependence of the first stage ($K_{U\leftrightarrow I}$) is virtually identical to that at 0.0 μM. This is of course consistent with our previous room temperature observations, whereby "prefolding" from U → I showed no sensitivity to the presence or absence of the cognate ligand. However, a much more dramatic effect of Co^{2+} on NiCo riboswitch folding is indicated by the rapid decrease of the second stage ($K_{I\leftrightarrow F}$) with increasing temperature, which now yields a strongly positive slope ($m > 0$) and a more negative intercept in the van't Hoff plot, corresponding to a substantial increase in both exothermicity ($\Delta H^0_{I\to F}$ = −44(6) vs −14(8) kcal/mol) and entropic loss ($\Delta S^0_{I\to F}$ = −146(21) vs −52(26) cal/mol/K) at 0.5 vs 0.0 μM. As a plausible physical picture, this would be consistent with the cognate ligand preferentially captured by a prefolded (I) vs unfolded (U) riboswitch via exothermic coordination of the Co^{2+}, resulting in a more highly ordered ligand-bound configuration and thus a significant loss in translational entropy.[57,58]

IIIE. Temperature-Dependent Folding Kinetics: Transition State Theory (TST) Analysis. Further information can be obtained from the corresponding temperature dependence of the forward/reverse kinetics, which can be deconstructed with Eyring/transition state theory (TST) analysis to yield isolated enthalpic and entropic contributions to the transition state barrier. Specifically, the thermodynamics of the transition state can be obtained from a standard Eyring plot of ln(k) vs $1/T$[31,34,41]

$$\ln(k) = -\frac{\Delta H^{\ddagger}}{R}\frac{1}{T} + \frac{\Delta S^{\ddagger}}{R} + \ln \nu \qquad (3)$$

In eq 3, $\Delta H^{\ddagger}$ and $\Delta S^{\ddagger}$ represent enthalpy and entropy differences between the transition state and the initial (or final) state, while ν represents an "attempt frequency" sampling the free energy barrier along the folding coordinate[59,60] and is often treated as a low-frequency skeletal vibration with $\nu \approx 10^{13}$ s^{-1}.[61,62] It is worth noting that $\Delta S^{\ddagger}$ depends only quite weakly (i.e., logarithmically) on the choice of ν, and furthermore, any differential (e.g., Co^{2+}-induced) changes in the transition state entropy ($\Delta\Delta S^{\ddagger}$) are rigorously independent of ν.

Eyring plots of eq 3 for the two conformational transformations U ↔ I and I ↔ F (forward and reverse) are presented in Figure 9 and reveal several interesting features.

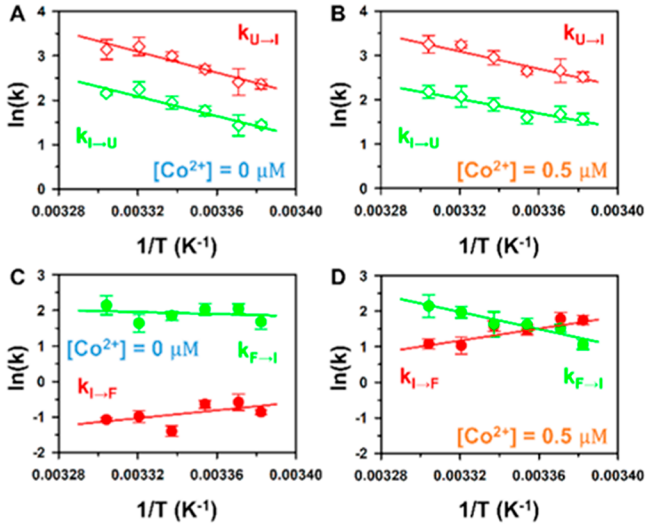

Figure 9. Temperature dependence of rate constants presented in Eyring plots: $k_{U\to I}$ (red empty diamonds) and $k_{I\to U}$ (green empty diamonds) at (A) $[Co^{2+}]$ = 0 μM and (B) $[Co^{2+}]$ = 0.5 μM; $k_{I\to F}$ (red solid circles) and $k_{F\to I}$ (green solid circles) at (C) $[Co^{2+}]$ = 0 μM and (D) $[Co^{2+}]$ = 0.5 μM. Data fits with linear regression yield detailed thermodynamic information (i.e., $\Delta H^{\ddagger}$ and $\Delta S^{\ddagger}$) by eq 3. Error bars represent 1σ standard deviations of the mean.

First of all, by visual comparison of Figures 9A and 9B, the plots for the U ↔ I kinetics indicate Co^{2+} to have only quite modest effects on the forward (folding) and reverse (unfolding) rate constants $k_{U\to I}$ and $k_{I\to U}$. This insensitivity to Co^{2+} in both the forward/reverse rate and equilibrium constants for this prefolding step implies negligible changes in

Table III. Thermodynamic Values Obtained from a van't Hoff Analysis of the Equilibrium Constant Data[a]

	$\Delta G^0_{U\to I}$ (kcal/mol)	$\Delta G^0_{I\to F}$ (kcal/mol)	$\Delta H^0_{U\to I}$ (kcal/mol)	$\Delta H^0_{I\to F}$ (kcal/mol)	$\Delta S^0_{U\to I}$ (cal/mol/K)	$\Delta S^0_{I\to F}$ (cal/mol/K)
$[Co^{2+}]$ = 0 μM	−0.54(4)	1.49(7)	1.4(13)	−14(8)	7(4)	−52(26)
$[Co^{2+}]$ = 0.5 μM	−0.56(9)	−0.41(10)	4.1(15)	−44(6)	16(4)	−146(21)

[a]Where ΔG^0 is calculated from K_{eq} at T = 22.5 °C. Error bars in parentheses represent 1σ uncertainties from the linear least squares fit.

https://dx.doi.org/10.1021/acs.jpcb.0c05625
J. Phys. Chem. B 2020, 124, 7348−7360

Table IV. Thermodynamic Values Obtained from an Eyring/TST Analysis[a]

	$\Delta H^{\ddagger}_{U\to I}$ (kcal/mol)	$\Delta H^{\ddagger}_{I\to U}$ (kcal/mol)	$\Delta H^{\ddagger}_{I\to F}$ (kcal/mol)	$\Delta H^{\ddagger}_{F\to I}$ (kcal/mol)	$\Delta S^{\ddagger}_{U\to I}$ (cal/mol/K)	$\Delta S^{\ddagger}_{I\to U}$ (cal/mol/K)	$\Delta S^{\ddagger}_{I\to F}$ (cal/mol/K)	$\Delta S^{\ddagger}_{F\to I}$ (cal/mol/K)
$[Co^{2+}] = 0\ \mu M$	23(3)	22(3)	−11(8)	3(6)	24(11)	18(11)	−98(27)	−46(22)
$[Co^{2+}] = 0.5\ \mu M$	20(2)	16(2)	−20(4)	24(4)	14(9)	−1(8)	−123(14)	24(13)

[a]Error bars in parentheses represent 1σ uncertainties from the linear least squares fit.

the first transition state barrier ($TS_{U\to I}$) with the cognate ligand. Indeed, the negative slopes observed for both $k_{U\to I}$ and $k_{I\to U}$ indicate a strong but equally endothermic process ($\Delta H^{\ddagger}_{U\to I}$ = 23(3) kcal/mol, $\Delta H^{\ddagger}_{I\to U}$ = 22(3) kcal/mol) to cross the transition barrier from either direction.

By way of contrast, the cognate ligand effects on the second stage I ↔ F conformational kinetics are clearly much more significant. In the absence of Co^{2+} (Figure 9C), both the forward ($k_{I\to F}$) and reverse ($k_{F\to I}$) folding rate constants depend only weakly on temperature, with slopes corresponding to $\Delta H^{\ddagger}_{I\to F}$ = −11(8) kcal/mol and $\Delta H^{\ddagger}_{F\to I}$ = 3(6) kcal/mol, respectively. Moreover, by eq 3, the entropic penalties of accessing the transition state are determined as $\Delta S^{\ddagger}_{I\to F}$ = −98(27) cal/mol/K and $\Delta S^{\ddagger}_{F\to I}$ = −46(22) cal/mol/K). However, in the presence of 0.5 μM Co^{2+}, the rate constant changes dramatically (cf. Figure 9C vs Figure 9D). The first effect is an increased slope in the rate constant for folding ($k_{I\to F}$) with decreasing experimental temperature, consistent with a more exothermic folding in the presence of the cognate ligand Co^{2+} ($\Delta H^{\ddagger}_{I\to F}$ = −20(4) vs −11(8) kcal/mol). This increased slope results in a more negative *y*-intercept, therefore predicting an even *greater entropic penalty* for Co^{2+}-induced folding ($\Delta S^{\ddagger}_{I\to F}$ = −123(14) vs −98(27) cal/mol/K). Simply summarized, the forward folding step (I → F) experiences a more significant entropic penalty ($-T\Delta\Delta S^{\ddagger}_{I\to F} > 0$) which is counterbalanced by increased enthalpic stabilization ($\Delta\Delta H^{\ddagger}_{I\to F} < 0$) in the presence of 0.5 μM Co^{2+}. The reverse folding step (F → I), on the other hand (see Figure 9D), now becomes noticeably more temperature-sensitive. From fits to eq 3, the riboswitch needs to cross a more significant enthalpic barrier to unfold ($\Delta H^{\ddagger}_{F\to I}$ = 24(4) vs 3(6) kcal/mol), with the effects strongly mitigated by entropic gain ($\Delta S^{\ddagger}_{F\to I}$ = 24(13) vs −46(22) cal/mol/K) in the presence and absence of the cognate ligand (see Table IV).

IV. DISCUSSION

IVA. Cations Facilitate Formation of a Prefolded NiCo Riboswitch Intermediate. The combination of FRET, time-correlated single-photon counting methods, and high NA confocal microscopy have permitted monitoring of the conformational kinetics of the NiCo riboswitch construct at the single-molecule level. The results indicate that folding proceeds via a two-step process between three conformations with three distinct E_{FRET} values (Figure 3), specifically identified as unfolded (U) and folded (F) states, with a stable "prefolded" intermediate conformation (I) directly along the U → F folding pathway (Figure 4). The cognate ligands (Co^{2+} and Ni^{2+}) are found to efficiently promote the formation of F from the prefolded intermediate I with submicromolar affinities by simultaneously increasing and decreasing $k_{I\to F}$ and $k_{F\to I}$, respectively. In sharp contrast, however, kinetic rates and overall equilibrium constants between the unfolded (U) and prefolded intermediate (I) conformations show zero dependence on cognate ligand concentrations up to micromolar levels. Finally, we find the first stage of folding/unfolding (U ↔ I) to be strongly stimulated by near physiological levels of monovalent (Na^+) and divalent (Mg^{2+}) cations (Figure 7). This collective behavior suggests that the NiCo riboswitch intermediate (I) is a prefolded structure stabilized by cations through charge neutralization and screening of the phosphate groups,[52,53] with an intermediate E_{FRET} value indicating that the helices are partially aligned toward the folded conformation due to preorganization of the junctional loop aptamer domain. Indeed, this would be consistent with previous studies, whereby a more fold-like conformation of riboswitches can be promoted by physiological levels of Mg^{2+} to increase the aptamer ligand affinity in a "fold-then-bind" mechansim.[29,36,37] Moreover, the present work has shown that monovalent cations (Na^+) exhibit similar stabilization effects for the intermediate state, requiring higher but still physiologically relevant concentrations. Such "fold-then-bind" behavior represents a classic example of conformational selection, whereby a biomolecule spontaneously samples many thermodynamically accessible configurations, but preferentially locking into an optimal "target" structure due to enhanced binding for the cognate ligand.[35] In this study, the prefolded NiCo riboswitch intermediate (I) is sufficiently long-lived to be identified by its distinct E_{FRET} value. As a novel result of the intermediate (I) being along the folding pathway and distinguishable from the unfolded (U) and folded states (F), we are able to follow the folding/binding process in single-molecule detail and thereby provide direct evidence for a "fold-then-bind" mechanism without any underlying kinetic model assumptions.[36,37]

IVB. Folding Is Induced by Ligand-Binding to the Conformational Intermediate. Ni^{2+} and Co^{2+} cognate ligands of the NiCo riboswitch have been shown to effectively promote conformational transformation from a prefolded intermediate I to the fully folded state F with submicromolar affinities. Furthermore, it achieves this while maintaining a fixed [U]/[I] ratio through cationic stabilization effects dominated by physiological monovalent (Na^+) and divalent (Mg^{2+}) salt conditions. As a function of increasing $[Co^{2+}]$ (Figure 5), the NiCo riboswitch is stabilized in the folded state (F) both by increasing the folding ($k_{I\to F}$) and decreasing the unfolding ($k_{F\to I}$) rate constant. The supralinear increase of $k_{I\to F}$ at low $[Co^{2+}]$ indicates the Co^{2+}-induced folding to be highly cooperative, consistent with previous in-line probing results.[16] The cooperativity for $k_{I\to F}$ is determined from a Hill analysis to be n = 3.1(11) (Table II), in good agreement with the three bound Co^{2+} ions resolved in the crystal data.[16] One should stress that Hill coefficients can differ from the number of bound ligands and are not always equivalent to the exact ligand stoichiometry.[63,64] Instead, the data indicate a consistency with complete folding (i.e., change in E_{FRET}) of the NiCo riboswitch upon association of the three Co^{2+} ions.

This cooperativity makes the NiCo riboswitch particularly sensitive to cognate ligand at concentrations in the transition region near $[Co^{2+}] \approx K_d$ = 0.32(4) μM and thus yielding a much sharper threshold response.[65,66] A cooperative Co^{2+}

https://dx.doi.org/10.1021/acs.jpcb.0c05625
J. Phys. Chem. B 2020, 124, 7348−7360

response of the NiCo riboswitch may therefore be advantageous by allowing cellular [Co^{2+}] to be maintained near K_d but where high cytotoxicity requires any additional Co^{2+} to be immediately removed.[6,7] Note that while the present K_d values are in quantitative agreement with the recent studies of NiCo-riboswitch-based fluorescent sensors titrated in citrate buffer,[67] they are roughly an order of magnitude lower (i.e., *more* sensitive) than previous in-line probing results.[16] We do not know the reason for these differences but can speculate that the presence of high [Mg^{2+}] in the in-line probing studies may interfere with ligand recognition/binding. Indeed, since Mg^{2+} is the dominant divalent cation in cells and is known to strongly interact with RNA, either synergy or competition between Mg^{2+} and the cognate ligands would be a natural possibility. This would suggest the value of future studies into Mg^{2+} cooperativity/anticooperativity effects on riboswitch response and metal ion toxicity.

The second cognate ligand Ni^{2+} promotes the NiCo riboswitch folding in a way qualitatively similar to Co^{2+}, with $k_{I\to F}$ and $k_{F\to I}$ systematically increasing and decreasing, respectively as a function of [Ni^{2+}] (Figure 6). There are, however, important differences between the two ligands. Specifically, the increase in $k_{I\to F}$ at low [Ni^{2+}] indicates a lower cooperativity (n = 1.8(10)) for Ni^{2+}-promoted folding, yet which is compensated by an even tighter ligand affinity (K_d = 0.26(7) μM) (Table II).[67] The results suggest that the NiCo riboswitch has evolved to trigger at lower levels of cognate ligand but more gradually toward removal of excess Ni^{2+}. A second difference in the NiCo riboswitch behavior can be seen in the saturation value of $k_{I\to F}$, which is nearly 3 times lower for Ni^{2+} than Co^{2+} and therefore predicts only ~50% of the folded population under saturating [Ni^{2+}] conditions. Such incomplete folding behavior, however, may not be characteristic of NiCo riboswitch *in vivo*, where more complete folding may be aided by molecular crowding and excluded volume interactions in the intracellular environment.[68,69]

IVC. Detailed Thermodynamics for Folding of the NiCo Riboswitch. NiCo riboswitch folding at the single-molecule level has been examined with temperature-controlled measurements to obtain detailed information on relative free energies (ΔG^0) for each of the three conformational states (U, I, and F) and two transition state barriers ($TS_{U\leftrightarrow I}$ and $TS_{I\leftrightarrow F}$) as well as the thermodynamic deconstruction of these free energies into enthalpic (ΔH) and entropic ($-T\Delta S$) contributions. These unusually rich free energy landscapes are presented in Figure 10, where the single arbitrary reference energy is chosen to be zero for the unfolded state (U). First, we focus on the limit of ligand-free folding, i.e. [Co^{2+}] = 0 (Figure 10A). In the prefolding transition (U → I), the system encounters an enthalpic barrier ($\Delta H^{\ddagger}_{U\to I}$ = 23(3) kcal/mol) that is only partially mitigated by small entropic gain corresponding to a free energy contribution $-T(\Delta S^{\ddagger}_{U\to I}) \approx$ −7(3) kcal/mol at T = 22.5 °C. Furthermore, after crossing the transition state ($TS_{U\leftrightarrow I}$), the riboswitch reaches the intermediate prefolded state (I) with a free energy surprisingly close to the unfolded conformation (U), despite a large 15 kcal/mol transition state barrier. The net near zero change in both $\Delta H^0_{U\to I}$ (1.4(13) kcal/mol) and $-T\Delta S^0_{U\to I}$ (−2.0(12) kcal/mol) would be consistent with the absence of significant cation association in the U → I step, which in contrast would be highly enthalpically favored and accompanied by large entropic loss due to reduced cation mobility. This suggests that the major structural transition from U → I instead involves

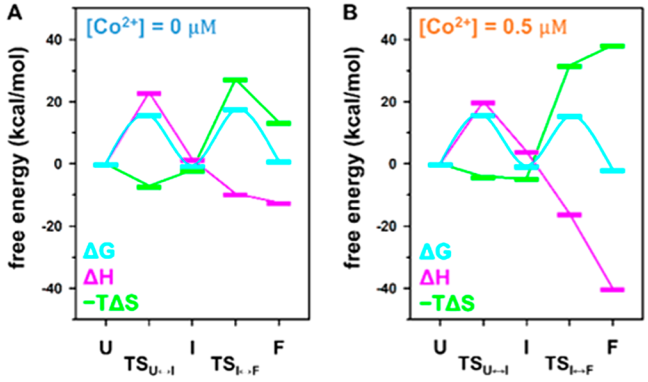

Figure 10. Detailed energy diagram of NiCo riboswitch folding at (A) [Co^{2+}] = 0 μM and (B) [Co^{2+}] = 0.5 μM, with the unfolded state (U) as reference zero (blue: ΔG, red: ΔH, green: $-T(\Delta S)$ at T = 22.5 °C).

modest rearrangement of the solvent (water) configuration and hydrogen bonding around the RNA junction that successively reorientates the four helices and results in the observed E_{FRET} change. A predominantly enthalpic barrier would thus be consistent with the simple physical picture that, during rearrangement, only some of the hydrogen bond structure is restored at the transition state ($TS_{U\leftrightarrow I}$). Furthermore, after crossing the transition barrier, hydrogen bond reformation enthalpically stabilizes the system and effectively brings down the free energy level of the intermediate state I, as illustrated in Figure 10A.

The second stage of folding (I → F) is more complex. In the absence of a cognate ligand (Figure 10A), the free energy transition state barrier ($TS_{I\to F}$) is dominated by entropic loss of the system ($-T(\Delta S^{\ddagger}_{I\to F})$ = 29(8) kcal/mol) partially mitigated by a relatively small exothermicity ($\Delta H^{\ddagger}_{I\to F}$ = −11(8) kcal/mol). Moreover, the final folded state F is stabilized by a further decrease in enthalpy ($\Delta H^0_{I\to F}$ = −14(8) kcal/mol) while destabilized by entropy loss ($-T(\Delta S^0_{I\to F})$ = 15(7) kcal/mol), with respect to the intermediate conformation (I). Such changes in the thermodynamics would be consistent with Coulomb repulsion of the phosphate groups partially neutralized by associated monovalent/divalent cations. We note that in the kinetic analysis, folding and unfolding between I and F conformations has been shown to be insensitive to Na^+/Mg^{2+} concentrations. While the cation association and neutralization are clearly indicated in the thermodynamic analysis, we therefore suspect the cation effects may saturate at relatively low concentrations. Alternatively stated, stabilizing cations are readily attracted to the four-way junction at relatively low concentrations. Therefore, cation stabilization effects and cation-insensitive folding are independently observed in thermodynamic and kinetic analysis, respectively.

In the presence of the cognate ligand [Co^{2+}] = 0.5 μM (Figure 10B), the free energy changes in the initial folding process (U → I) are quite similar to those at [Co^{2+}] = 0 μM (see also Tables III and IV). This is again consistent with our previous observation (Figure 5A) of an insensitivity in the U → I folding pathway to Co^{2+}. The more dramatic Co^{2+} effects are seen in the (I ↔ F) transition between the prefolded and fully folded state. At the second transition state ($TS_{I\leftrightarrow F}$), the presence of Co^{2+} results in an increased entropic barrier ($-T(\Delta S^{\ddagger}_{I\to F})$ = 36(4) vs 29(8) kcal/mol at [Co^{2+}] = 0), accompanied by a 2× greater enthalpic stabilization ($\Delta H^{\ddagger}_{I\to F}$ =

https://dx.doi.org/10.1021/acs.jpcb.0c05625
J. Phys. Chem. B 2020, 124, 7348−7360

−20(4) vs −11(8) kcal/mol). Furthermore, the Co^{2+} effects are even stronger for the overall I → F changes in free energy due to enthalpy ($\Delta H^0_{I\to F}$ = −44(6) vs −14(8) kcal/mol) and entropy ($-T(\Delta S^0_{I\to F})$ = 43(6) vs 15(7) kcal/mol) for 0.5 and 0.0 μM, respectively. Both this increased entropic penalty and enthalpic stabilization along the folding coordinate are consistent with strong binding of the cognate ligand to the binding site to form a more ordered structure with loss in mobility.[58] In contrast with the monovalent/divalent cation effects at $[Co^{2+}] = 0$, the greater enthalpic stabilization of Co^{2+} due to the metal coordination overcomes the entropic loss, resulting an overall free energy change in slight favor of the folded (F) conformation ($\Delta G^0_{I\to F}$ = −0.41 vs +1.49(7) kcal/mol at $[Co^{2+}] = 0$). In fact, such thermodynamic shifts induced by ligand association are routinely observed in both ligand-binding protein[70] and nucleic acid[34,71] systems. Our results thus provide additional thermodynamic support for cognate ligand Co^{2+}-binding to the prefolded conformation (I) directly promoting and stabilizing the folded structure (F) in a "fold-then-bind" conformational selection mechanism.

As a parting comment, it is noteworthy that the enthalpic (ΔH^0) and entropic ($-T(\Delta S^0)$) contributions to the overall free energy change are large in magnitude and of opposing signs. Such a counterbalance between the enthalpic/entropic effects is known as entropy−enthalpy compensation.[58,72] In folding of the NiCo riboswitch, such enthalpy−entropy compensation effects are seen to occur multiple times, as highlighted in Figure 10 by the relatively modest shifts in ΔG^0 values contrasting with the order of magnitude larger ΔH^0 and $-T\Delta S^0$ values. As one example, the free energy $\Delta G^0_{I\to F}$ for I → F folding in the presence of Co^{2+} is only −0.41(10) kcal/mol, despite the fact that each of the entropic penalties and enthalpic stabilization effects are larger by 2 orders of magnitude (>40 kcal/mol). Similarly, in the absence of Co^{2+}, $\Delta G^0_{I\to F}$ is +1.49(7) kcal/mol, while the enthalpic stabilization as well as entropic destabilization components are 10× higher (>15 kcal/mol). Such a biological propensity to achieve nearly equally balanced free energy contributions in $-T\Delta S^0$ and ΔH^0 for conformational change offers one way to modulate the temperature sensitivity of RNA folding and conformational stability of a biologically competent species with only small changes in the overall free energy ΔG^0.

V. SUMMARY AND CONCLUSION

The present work reports on the single-molecule kinetics and thermodynamics of folding of the NiCo ribowitch construct as a function of (i) cognate ligand (Ni^{2+}, Co^{2+}), (ii) background monovalent (Na^+) and divalent (Mg^{2+}) concentrations, and (iii) temperature (T = 20 to 30K). Although the aptamer domain structure of the NiCo riboswitch is built on a four-way junction with no long-range tertiary stem−stem or loop−loop interactions, evidence from the present single-molecule study reveals it to be more complex and kinetically interesting than a simple two-state folder. Specifically, the NiCo riboswitch has been shown to dynamically fluctuate between three stable conformations (unfolded U, folded F, and intermediate I) and exhibit three distinct E_{FRET} values. Of particular relevance, the overwhelming majority (>98%) of all transitions between unfolded (U) and folded (F) conformations sample this third conformation (I), which therefore acts as a long-lived, prefolded intermediate through which overall folding proceeds by two distinct steps (U → I and I → F). This intermediate I proves particularly crucial for selective cognate ligand recognition and ligand-induced folding, as clearly evidenced by the fact that Ni^{2+}/Co^{2+} strongly promotes the I → F folding step, while Mg^{2+}/Na^+ has little effect even at 3−5 orders of magnitude higher concentrations. As a result, the first stage of this NiCo riboswitch folding (U → I) can be facilitated by $[Na^+]$ and $[Mg^{2+}]$ present at physiological levels, whereas the second stage of folding is controlled with high selectivity by submicromolar concentrations of the cognate ligand. The overall folding pathway thus follows a classic "fold-then-bind" conformational selection mechanism, whereby the binding site on the prefolded intermediate captures cognate ligands with high selectivity and thereby stabilizes the overall folding event. Furthermore, both Ni^{2+} and Co^{2+} are shown from a Hill analysis to *cooperatively* promote folding of the NiCo riboswitch, with cation selective signatures in Hill cooperativity, K_d affinity, and saturation kinetics. As a result, these unique signatures could offer the NiCo riboswitch a mechanism for discriminating between Ni^{2+} and Co^{2+} to optimize gene-regulation efficiency and *in vivo* management of metal ion cytotoxicity. Finally, detailed free energy landscapes have been reconstructed from van't Hoff and Eyring analysis of the temperature-dependent equilibrium and kinetic data. The results highlight a complete insensitivity of the first prefolding step (U → $TS_{U\leftrightarrow I}$ → I) to the cognate ligand, with both dramatic entropy−enthalpy compensation and cognate ligand sensitivity effects along the second step (I → $TS_{I\leftrightarrow F}$ → F) for folding the NiCo riboswitch into a biochemically competent shape.

AUTHOR INFORMATION

Corresponding Author

David J. Nesbitt − *JILA, National Institute of Standards and Technology and University of Colorado, Boulder, Colorado 80309, United States; Department of Chemistry and Department of Physics, University of Colorado, Boulder, Colorado 80309, United States;* orcid.org/0000-0001-5365-1120; Email: djn@jila.colorado.edu

Author

Hsuan-Lei Sung − *JILA, National Institute of Standards and Technology and University of Colorado, Boulder, Colorado 80309, United States; Department of Chemistry, University of Colorado, Boulder, Colorado 80309, United States*

Complete contact information is available at: https://pubs.acs.org/10.1021/acs.jpcb.0c05625

Notes

The authors declare no competing financial interest.

ACKNOWLEDGMENTS

Primary support for this work has been through the National Science Foundation under grant CHE-1665271 from the Chemical, Structure, Dynamics and Mechanisms-A Program, with additional support for development of the confocal apparatus from PHY-1734006 (Physics Frontier Center Program). We would also like to acknowledge early seed contributions by the W. M. Keck Foundation Initiative in RNA Sciences at the University of Colorado, Boulder, and well as transitional support from the Air Force Office of Scientific Research (FA9550-15-1-0090). We also would like to acknowledge helpful discussions with David Nicholson, Andrea Marton, and Prof. Erik Holmstrom (University of Kansas).

https://dx.doi.org/10.1021/acs.jpcb.0c05625
J. Phys. Chem. B 2020, 124, 7348−7360

REFERENCES

(1) Barrick, J. E.; Breaker, R. R. The Distributions, Mechanisms, and Structures of Metabolite-Binding Riboswitches. *Genome Biol.* **2007**, *8*, R239.

(2) Garst, A. D.; Edwards, A. L.; Batey, R. T. Riboswitches: Structures and Mechanisms. *Cold Spring Harbor Perspect. Biol.* **2011**, *3*, a003533.

(3) Nudler, E.; Mironov, A. S. The Riboswitch Control of Bacterial Metabolism. *Trends Biochem. Sci.* **2004**, *29*, 11−17.

(4) Winkler, W. C.; Breaker, R. R. Regulation of Bacterial Gene Expression by Riboswitches. *Annu. Rev. Microbiol.* **2005**, *59*, 487−517.

(5) McCown, P. J.; Corbino, K. A.; Stav, S.; Sherlock, M. E.; Breaker, R. R. Riboswitch Diversity and Distribution. *RNA* **2017**, *23*, 995−1011.

(6) Valko, M.; Morris, H.; Cronin, M. T. D. Metals, Toxicity and Oxidative Stress. *Curr. Med. Chem.* **2005**, *12*, 1161−1208.

(7) Jaishankar, M.; Tseten, T.; Anbalagan, N.; Mathew, B. B.; Beeregowda, K. N. Toxicity, Mechanism and Health Effects of Some Heavy Metals. *Interdiscip. Toxicol.* **2014**, *7*, 60−72.

(8) Andreini, C.; Bertini, I.; Cavallaro, G.; Holliday, G. L.; Thornton, J. M. Metal Ions in Biological Catalysis: From Enzyme Databases to General Principles. *J. Biol. Inorg. Chem.* **2008**, *13*, 1205−1218.

(9) Hausinger, R. P. Nickel Utilization by Microorganisms. *Microbiol. Rev.* **1987**, *51*, 22−42.

(10) Chen, P. R.; He, C. Selective Recognition of Metal Ions by Metalloregulatory Proteins. *Curr. Opin. Chem. Biol.* **2008**, *12*, 214−221.

(11) Reyes-Caballero, H.; Campanello, G. C.; Giedroc, D. P. Metalloregulatory Proteins: Metal Selectivity and Allosteric Switching. *Biophys. Chem.* **2011**, *156*, 103−114.

(12) Pyle, A. Metal Ions in the Structure and Function of RNA. *J. Biol. Inorg. Chem.* **2002**, *7*, 679−690.

(13) Saunders, A. M.; DeRose, V. J. Beyond Mg^{2+}: Functional Interactions between RNA and Transition Metals. *Curr. Opin. Chem. Biol.* **2016**, *31*, 153−159.

(14) Price, I. R.; Gaballa, A.; Ding, F.; Helmann, J. D.; Ke, A. Mn^{2+}-Sensing Mechanisms of *Yybp-Ykoy* Orphan Riboswitches. *Mol. Cell* **2015**, *57*, 1110−1123.

(15) Dambach, M.; Sandoval, M.; Updegrove, T. B.; Anantharaman, V.; Aravind, L.; Waters, L. S.; Storz, G. The Ubiquitous *Yybp-Ykoy* Riboswitch Is a Manganese-Responsive Regulatory Element. *Mol. Cell* **2015**, *57*, 1099−1109.

(16) Furukawa, K.; Ramesh, A.; Zhou, Z.; Weinberg, Z.; Vallery, T.; Winkler, W. C.; Breaker, R. R. Bacterial Riboswitches Cooperatively Bind Ni^{2+} or Co^{2+} Ions and Control Expression of Heavy Metal Transporters. *Mol. Cell* **2015**, *57*, 1088−1098.

(17) Anton, A.; Große, C.; Reißmann, J.; Pribyl, T.; Nies, D. H. CzcD Is a Heavy Metal Ion Transporter Involved in Regulation of Heavy Metal Resistance in *Ralstonia* Sp. Strain CH34. *J. Bacteriol.* **1999**, *181*, 6876−6881.

(18) Große, C.; Anton, A.; Hoffmann, T.; Franke, S.; Schleuder, G.; Nies, D. H. Identification of a Regulatory Pathway That Controls the Heavy-Metal Resistance System Czc Via Promoter czcNp in *Ralstonia Metallidurans*. *Arch. Microbiol.* **2004**, *182*, 109−118.

(19) Bouzat, J. L.; Hoostal, M. J. Evolutionary Analysis and Lateral Gene Transfer of Two-Component Regulatory Systems Associated with Heavy-Metal Tolerance in Bacteria. *J. Mol. Evol.* **2013**, *76*, 267−279.

(20) Frieda, K. L.; Block, S. M. Direct Observation of Cotranscriptional Folding in an Adenine Riboswitch. *Science* **2012**, *338*, 397−400.

(21) Watters, K. E.; Strobel, E. J.; Yu, A. M.; Lis, J. T.; Lucks, J. B. Cotranscriptional Folding of a Riboswitch at Nucleotide Resolution. *Nat. Struct. Mol. Biol.* **2016**, *23*, 1124−1131.

(22) Tolić-Nørrelykke, S. F.; Engh, A. M.; Landick, R.; Gelles, J. Diversity in the Rates of Transcript Elongation by Single RNA Polymerase Molecules. *J. Biol. Chem.* **2004**, *279*, 3292−3299.

(23) Wickiser, J. K.; Winkler, W. C.; Breaker, R. R.; Crothers, D. M. The Speed of RNA Transcription and Metabolite Binding Kinetics Operate an Fmn Riboswitch. *Mol. Cell* **2005**, *18*, 49−60.

(24) Lemay, J.-F.; Desnoyers, G.; Blouin, S.; Heppell, B.; Bastet, L.; St-Pierre, P.; Massé, E.; Lafontaine, D. A. Comparative Study between Transcriptionally- and Translationally-Acting Adenine Riboswitches Reveals Key Differences in Riboswitch Regulatory Mechanisms. *PLoS Genet.* **2011**, *7*, e1001278.

(25) Lutz, B.; Faber, M.; Verma, A.; Klumpp, S.; Schug, A. Differences between Cotranscriptional and Free Riboswitch Folding. *Nucleic Acids Res.* **2014**, *42*, 2687−2696.

(26) Zhuang, X.; Bartley, L. E.; Babcock, H. P.; Russell, R.; Ha, T.; Herschlag, D.; Chu, S.; Single-Molecule, A. Study of RNA Catalysis and Folding. *Science* **2000**, *288*, 2048−2051.

(27) Roy, R.; Hohng, S.; Ha, T. A Practical Guide to Single-Molecule FRET. *Nat. Methods* **2008**, *5*, 507−516.

(28) Guo, Z.; Karunatilaka, K. S.; Rueda, D. Single-Molecule Analysis of Protein-Free U2−U6 snRNAs. *Nat. Struct. Mol. Biol.* **2009**, *16*, 1154−1159.

(29) McCluskey, K.; Boudreault, J.; St-Pierre, P.; Perez-Gonzalez, C.; Chauvier, A.; Rizzi, A.; Beauregard, P. B.; Lafontaine, D. A.; Penedo, J. C. Unprecedented Tunability of Riboswitch Structure and Regulatory Function by Sub-Millimolar Variations in Physiological Mg^{2+}. *Nucleic Acids Res.* **2019**, *47*, 6478−6487.

(30) Lu, M.; Ma, X.; Castillo-Menendez, L. R.; Gorman, J.; Alsahafi, N.; Ermel, U.; Terry, D. S.; Chambers, M.; Peng, D.; Zhang, B.; et al. Associating HIV-1 Envelope Glycoprotein Structures with States on the Virus Observed by smFRET. *Nature* **2019**, *568*, 415−419.

(31) Fiore, J. L.; Holmstrom, E. D.; Nesbitt, D. J. Entropic Origin of Mg^{2+}-Facilitated RNA Folding. *Proc. Natl. Acad. Sci. U. S. A.* **2012**, *109*, 2902−2907.

(32) Nicholson, D. A.; Sengupta, A.; Sung, H.-L.; Nesbitt, D. J. Amino Acid Stabilization of Nucleic Acid Secondary Structure: Kinetic Insights from Single-Molecule Studies. *J. Phys. Chem. B* **2018**, *122*, 9869−9876.

(33) Holmstrom, E. D.; Nesbitt, D. J. Biophysical Insights from Temperature-Dependent Single-Molecule Förster Resonance Energy Transfer. *Annu. Rev. Phys. Chem.* **2016**, *67*, 441−465.

(34) Sung, H.-L.; Nesbitt, D. J. Novel Heat-Promoted Folding Dynamics of the Yybp-Ykoy Manganese Riboswitch: Kinetic and Thermodynamic Studies at the Single-Molecule Level. *J. Phys. Chem. B* **2019**, *123*, 5412−5422.

(35) Vogt, A. D.; Pozzi, N.; Chen, Z.; Di Cera, E. Essential Role of Conformational Selection in Ligand Binding. *Biophys. Chem.* **2014**, *186*, 13−21.

(36) Suddala, K. C.; Wang, J.; Hou, Q.; Walter, N. G. Mg^{2+} Shifts Ligand-Mediated Folding of a Riboswitch from Induced-Fit to Conformational Selection. *J. Am. Chem. Soc.* **2015**, *137*, 14075−14083.

(37) Sung, H.-L.; Nesbitt, D. J. Single-Molecule FRET Kinetics of the Mn^{2+} Riboswitch: Evidence for Allosteric Mg^{2+} Control of "Induced-Fit" Vs "Conformational Selection" Folding Pathways. *J. Phys. Chem. B* **2019**, *123*, 2005−2015.

(38) Serganov, A.; Yuan, Y.-R.; Pikovskaya, O.; Polonskaia, A.; Malinina, L.; Phan, A. T.; Hobartner, C.; Micura, R.; Breaker, R. R.; Patel, D. J. Structural Basis for Discriminative Regulation of Gene Expression by Adenine- and Guanine-Sensing Mrnas. *Chem. Biol.* **2004**, *11*, 1729−1741.

(39) Garst, A. D.; Héroux, A.; Rambo, R. P.; Batey, R. T. Crystal Structure of the Lysine Riboswitch Regulatory mRNA Element. *J. Biol. Chem.* **2008**, *283*, 22347−22351.

(40) Serganov, A.; Huang, L.; Patel, D. J. Coenzyme Recognition and Gene Regulation by a Flavin Mononucleotide Riboswitch. *Nature* **2009**, *458*, 233−237.

(41) Sengupta, A.; Sung, H.-L.; Nesbitt, D. J. Amino Acid Specific Effects on RNA Tertiary Interactions: Single-Molecule Kinetic and Thermodynamic Studies. *J. Phys. Chem. B* **2016**, *120*, 10615−10627.

(42) Holmstrom, E. D.; Nesbitt, D. J. Single-Molecule Fluorescence Resonance Energy Transfer Studies of the Human Telomerase RNA Pseudoknot: Temperature-/Urea-Dependent Folding Kinetics and Thermodynamics. *J. Phys. Chem. B* **2014**, *118*, 3853−3863.

https://dx.doi.org/10.1021/acs.jpcb.0c05625
J. Phys. Chem. B 2020, 124, 7348−7360

(43) Sung, H.-L.; Nesbitt, D. J. DNA Hairpin Hybridization under Extreme Pressures: A Single-Molecule FRET Study. *J. Phys. Chem. B* **2020**, *124*, 110−120.
(44) Fiore, J. L.; Holmstrom, E. D.; Fiegland, L. R.; Hodak, J. H.; Nesbitt, D. J. The Role of Counterion Valence and Size in GAAA Tetraloop−Receptor Docking/Undocking Kinetics. *J. Mol. Biol.* **2012**, *423*, 198−216.
(45) Qin, F.; Auerbach, A.; Sachs, F. A Direct Optimization Approach to Hidden Markov Modeling for Single Channel Kinetics. *Biophys. J.* **2000**, *79*, 1915−1927.
(46) Andrec, M.; Levy, R. M.; Talaga, D. S. Direct Determination of Kinetic Rates from Single-Molecule Photon Arrival Trajectories Using Hidden Markov Models. *J. Phys. Chem. A* **2003**, *107*, 7454−7464.
(47) Schröder, G. F.; Grubmüller, H. Maximum Likelihood Trajectories from Single Molecule Fluorescence Resonance Energy Transfer Experiments. *J. Chem. Phys.* **2003**, *119*, 9920−9924.
(48) McKinney, S. A.; Joo, C.; Ha, T. Analysis of Single-Molecule FRET Trajectories Using Hidden Markov Modeling. *Biophys. J.* **2006**, *91*, 1941−1951.
(49) Forsén, S.; Linse, S. Cooperativity: Over the Hill. *Trends Biochem. Sci.* **1995**, *20*, 495−497.
(50) Schroeder, K. T.; Daldrop, P.; Lilley, D. M.J. RNA Tertiary Interactions in a Riboswitch Stabilize the Structure of a Kink Turn. *Structure* **2011**, *19*, 1233−1240.
(51) Fiegland, L. R.; Garst, A. D.; Batey, R. T.; Nesbitt, D. J. Single-Molecule Studies of the Lysine Riboswitch Reveal Effector-Dependent Conformational Dynamics of the Aptamer Domain. *Biochemistry* **2012**, *51*, 9223−9233.
(52) Draper, D. E.; Grilley, D.; Soto, A. M. Ions and RNA Folding. *Annu. Rev. Biophys. Biomol. Struct.* **2005**, *34*, 221−243.
(53) Woodson, S. A. Metal Ions and RNA Folding: A Highly Charged Topic with a Dynamic Future. *Curr. Opin. Chem. Biol.* **2005**, *9*, 104−109.
(54) Goody, T. A.; Melcher, S. E.; Norman, D. G.; Lilley, D. M. J. The Kink-Turn Motif in RNA Is Dimorphic, and Metal Ion-Dependent. *RNA* **2004**, *10*, 254−264.
(55) Hohng, S.; Wilson, T. J.; Tan, E.; Clegg, R. M.; Lilley, D. M. J.; Ha, T. Conformational Flexibility of Four-Way Junctions in RNA. *J. Mol. Biol.* **2004**, *336*, 69−79.
(56) Holmstrom, E. D.; Fiore, J. L.; Nesbitt, D. J. Thermodynamic Origins of Monovalent Facilitated RNA Folding. *Biochemistry* **2012**, *51*, 3732−3743.
(57) Irudayam, S. J.; Henchman, R. H. Entropic Cost of Protein−Ligand Binding and Its Dependence on the Entropy in Solution. *J. Phys. Chem. B* **2009**, *113*, 5871−5884.
(58) Zhou, H.-X.; Gilson, M. K. Theory of Free Energy and Entropy in Noncovalent Binding. *Chem. Rev.* **2009**, *109*, 4092−4107.
(59) Kramers, H. A. Brownian Motion in a Field of Force and the Diffusion Model of Chemical Reactions. *Physica* **1940**, *7*, 284−304.
(60) Grote, R. F.; Hynes, J. T. The Stable States Picture of Chemical Reactions. II. Rate Constants for Condensed and Gas Phase Reaction Models. *J. Chem. Phys.* **1980**, *73*, 2715−2732.
(61) Szabo, A.; Schulten, K.; Schulten, Z. First Passage Time Approach to Diffusion Controlled Reactions. *J. Chem. Phys.* **1980**, *72*, 4350−4357.
(62) Zwanzig, R.; Szabo, A.; Bagchi, B. Levinthal's Paradox. *Proc. Natl. Acad. Sci. U. S. A.* **1992**, *89*, 20−22.
(63) Weiss, J. N. The Hill Equation Revisited: Uses and Misuses. *FASEB J.* **1997**, *11*, 835−841.
(64) Leipply, D.; Draper, D. E. Dependence of RNA Tertiary Structural Stability on Mg^{2+} Concentration: Interpretation of the Hill Equation and Coefficient. *Biochemistry* **2010**, *49*, 1843−1853.
(65) Goldbeter, A.; Koshland, D. E. An Amplified Sensitivity Arising from Covalent Modification in Biological Systems. *Proc. Natl. Acad. Sci. U. S. A.* **1981**, *78*, 6840−6844.
(66) Ralston, D. M.; O'Halloran, T. V. Ultrasensitivity and Heavy-Metal Selectivity of the Allosterically Modulated Merr Transcription Complex. *Proc. Natl. Acad. Sci. U. S. A.* **1990**, *87*, 3846−3850.
(67) Xu, J.; Cotruvo, J. A. The Czcd (Nico) Riboswitch Responds to Iron(II). *Biochemistry* **2020**, *59*, 1508−1516.
(68) Minton, A. P. Macromolecular Crowding and Molecular Recognition. *J. Mol. Recognit.* **1993**, *6*, 211−214.
(69) Zhou, H.-X.; Rivas, G.; Minton, A. P. Macromolecular Crowding and Confinement: Biochemical, Biophysical, and Potential Physiological Consequences. *Annu. Rev. Biophys.* **2008**, *37*, 375−397.
(70) Reynolds, C. H.; Holloway, M. K. Thermodynamics of Ligand Binding and Efficiency. *ACS Med. Chem. Lett.* **2011**, *2*, 433−437.
(71) Marchand, A.; Rosu, F.; Zenobi, R.; Gabelica, V. Thermal Denaturation of DNA G-Quadruplexes and Their Complexes with Ligands: Thermodynamic Analysis of the Multiple States Revealed by Mass Spectrometry. *J. Am. Chem. Soc.* **2018**, *140*, 12553−12565.
(72) Gallicchio, E.; Kubo, M. M.; Levy, R. M. Entropy−Enthalpy Compensation in Solvation and Ligand Binding Revisited. *J. Am. Chem. Soc.* **1998**, *120*, 4526−4527.

https://dx.doi.org/10.1021/acs.jpcb.0c05625
J. Phys. Chem. B 2020, 124, 7348−7360